Young's modulus of thin SmS films measured by nanoindentation and laser acoustic wave

H. Zhang, M. Stewart, F. De Luca, P.F. Smet, A. Sousanis, D. Poelman, I. Rungger, M. Gee

PII: S0257-8972(21)00602-2

DOI: https://doi.org/10.1016/j.surfcoat.2021.127428

Reference: SCT 127428

To appear in: *Surface & Coatings Technology*

Please cite this article as: H. Zhang, M. Stewart, F. De Luca, et al., Young's modulus of thin SmS films measured by nanoindentation and laser acoustic wave, *Surface & Coatings Technology* (2021), https://doi.org/10.1016/j.surfcoat.2021.127428

Young's modulus of thin SmS films measured by nanoindentation and laser acoustic wave

H Zhang[1*], M Stewart[1], F De Luca[1], P F Smet[2], A Sousanis[2], D Poelman[2], I Rungger[1], M Gee[1*]

1 National Physical Laboratory, Hampton Road, Teddington, Middlesex, TW11 0LW, UK

2 LumiLab, Dept. Solid State Sciences, Ghent University, Krijgslaan 281/S1, 9000 Gent, Belgium

* Contact: Hannah.zhang@npl.co.uk; Mark.gee@npl.co.uk

Abstract

High quality phase pure samarium sulphide (SmS) thin films with low surface roughness were prepared by electron beam evaporation using a samarium metal source in an H_2S atmosphere. SmS shows a strong piezoresistive response due to a phase transition between a semiconducting and metallic state, which can be employed in piezo-electronic devices and stress sensing. Measurement of fundamental mechanical properties such as Young's modulus is thus a major objective to assess the elastic behaviour of SmS under external stress. Nanoindentation was used to measure the elastic modulus of thin semiconducting films with nominal thickness of 100 nm, 200 nm and 400 nm on silicon substrate at different loads. The indentation results were fitted to a modified King's model to exclude the effect of the substrate, giving Young's moduli of the films in the range of 79-82 GPa, consistent with measurements with a Laser Surface Acoustic Wave system (LAwave) and results from literature.

Key words: Samarium sulphide, Thin film, Nanoindentation, LAwave, Young's modulus

1. Introduction

Samarium sulphide (SmS) exhibits an isostructural first-order phase transition from the semiconducting to the metallic state at a hydrostatic pressure of about 650 MPa at room temperature [1]. The moderate conditions (pressure and temperature) required for switching, and the possibility to modify the material to make the transition reversible, make SmS an important and unique material for potential applications such as non-volatile memory devices, stress/strain sensors, pressure related electronics and so on [2]. The switching process from semiconducting to metallic state is a volume collapse which can be reversed by thermal annealing. The basic properties and switching characteristics of SmS, and the way to monitor these properties, have been reviewed in Reference [2]. For real-world applications, high quality SmS thin films are required, with stringent requirements on their electrical and mechanical properties, but the physics of contact-induced deformation of thin films has not been fully investigated [3]. The size of SmS in a piezoelectronic transistor device is in the sub-micrometre range [3, 4], as required by the IT industry. As the mechanical properties of small structures may be significantly different from those of bulk material (i.e. a size effect) [5], there is a need to study the mechanical properties of SmS at the appropriate scale.

Although the indentation response of a thin film on a substrate is a complex function of the elastic and plastic properties of both the film and substrate, nanoindentation is a promising method for obtaining mechanical property information of thin films for input to theoretical and computational analysis [5-14]. In order to measure 'film-only' properties, a commonly used approach is to limit the indentation depth to less than 10 % of the film thickness, although depending on the properties of the film and substrate, the depth limit varies, with values reported between 5 % and 35 % of the film thickness [11, 15]. Experimentally, this

thickness ratio rule is applicable for films with a thickness greater than one micrometre. Several computational models were successfully demonstrated and applied to determine mechanical properties of thin films with thickness of 100 nm or lower, with both spherical and pyramidal indenters [5, 14].

For film-only properties of SmS thin films, a pyramidal indenter is used to measure the local Young's modulus. A test protocol was developed for the measurement of both metallic and non-metallic materials in ISO standard (BS EN ISO 14577-4: 2016) [16], where the elastic modulus of coatings was obtained by taking a series of measurements at different indentation depths. In the case of soft/ductile coatings like SmS, indentation force or displacement and indenter geometry should be chosen such that a larger radius indenter is used, which increases the difficulty to determine the surface contact point due to the imperfections of the indenter. For the measurement of small surface area (i.e. for the real application, the size of SmS is in sub-micro or nano metre scale [3]) and the analysis of the unloading curve with Oliver & Pharr method [15], the area of the test piece needs to be much larger than the area of indent based on the Hertz contact theory. Therefore, a pyramidal (sharp) indenter is used in this work. Saha and Nix [11] modified King's model [12] (where Young's modulus is measured with flat punch indenters), to adapt it to three-face pyramidal indenters, and different material systems irrespective of the effects of pile-up or sink-in such as observed for Cu and ultrahard alloys thin films [5, 17, 18]. Furthermore, laser surface acoustic wave measurements (LAwave technique) were also used to investigate the elastic properties of the films, allowing for a greater area to be analysed (on the order of a few millimetres square) and assessing their degree of uniformity.

2. Methods

Samarium sulphide (SmS) thin films in semiconducting state were prepared by electron beam evaporation using a samarium metal source in an H_2S atmosphere, on silicon substrate at 250 ˚C [19]. Thin films with different nominal thickness of 100, 200 and 400 nm were deposited, and the actual thickness measured along the cross section with a Scanning Electron Microscope (SEM) was 102, 197 and 424 nm, respectively. The surface roughness of the thin films was measured with an atomic force microscope (AFM, M5, Park, South Korea)), operated in contact mode.

FIGURE 1 [HERE]

Figure 1 shows a schematic of an indentation and the corresponding load-displacement curve. In the Oliver-Pharr method, the elastic solution for the indentation of an isotropic half space is used to relate the contact stiffness S and the projected contact area $A(h_c)$ between the indenter and half space to the reduced modulus (E_r) of a homogeneous material, $E_r = \frac{S\sqrt{\pi}}{2\sqrt{A}}$. In an elasto-plastic indentation, h_c is contact depth, S is measured as the derivative of the indentation load P with respect to the elastic displacement upon unloading (as shown in Figure 1 (b)). The elastic unloading from a plastic impression is equivalent to the elastic indentation of a flat surface by an effective punch, the shape of which is determined by the plastic properties of the material. For an isotropic material with a Poisson's ratio v, Young's modulus (E) can be calculated from $\frac{1}{E_r} = \frac{1-v_i^2}{E_i} + \frac{1-v^2}{E}$, where E_i and v_i are the Young modulus (1141 GPa) and Poisson's ratio (0.07) of the diamond indenter, respectively.

In this study, nanoindentation on thin films was performed using an Ultra Nanoindentation Tester (UNHT^3, Anton Paar, Austria), equipped with a diamond cube corner indenter, of

which the area function was calibrated with certified reference materials. Nanoindentation experiments were conducted at varying loads, namely, 0.05, 0.1, 0.2 0.4, 0.6, 0.8. 1.2 and 2 mN, in load-control, while applying and removing the load within 30 s. At the maximum load, a dwell period of 60 seconds was maintained before unloading, as well as another dwell period of 60 s at 90 % of unloading for thermal drift correction. At least 10 indents were performed at each load on each specimen, with an indent spacing of at least 10 μm. A spherical indenter with a radius of 4.2 μm was used to investigate the effect of surface contact on certified reference materials (average roughness Ra is < 2 nm, as determined by AFM) and thin films. Multiload cycles with Berkovich indenter were also carried out to compare the fitting results on the 400 nm thick SmS film. Furthermore, an attempt was made to measure Young's modulus of metallic phase SmS, after rubbing the 400 nm thin film with a small force with a pair of plastic tweezers to trigger the phase transition [19]. However, the measurement was not successful despite the metallic phase was obtained, due to the uneven surface caused by this uncontrollable process.

For the laser surface acoustic wave measurements, 3 out of 4 parameters among the Young's modulus (E), Poisson's ratio (ν), mass density (ρ) and layer thickness (t) need to be known before the fourth parameter can be calculated [20-22]. The computation is based on the velocity of a surface (c) wave in a homogeneous isotropic material, taken from the theory of the measurement as.

$$c = \frac{0.87+1.12\nu}{1+\nu}\sqrt{\frac{E}{2\rho(1+\nu)}} \quad (1)$$

For a homogeneous material, the velocity does not depend on frequency, and the shape of the pulse at different distances from the laser focus is identical, merely shifted in time. If there is a coating on the sample, the stiffness and density of the surface are changed, and the wave motion is altered. The lower frequency waves penetrate deeper into the substrate and are

indicative of the substrate, and the higher frequency are closer to the surface and carry information on the film. To investigate this the system makes measurements of the transmitted pulse at different distances along the sample, where increasing the separation distance causes the pulse to become broader (i.e. the dispersion). As there is no information on the shape of the pulse introduced, and the frequency response of the detector, the system works on the difference between two curves (pulse) generated at two distances (x_1 and x_2) between the laser focus line and transducer to measure the phase velocity, not the absolute impulse response of the transducer.

The two pulses are Fourier transformed and cross correlated. From the cross correlated pulses at each position the software can construct the dispersion curve in the form of the phase velocity as a function of frequency, based on the relation

$$c = \frac{2\pi f(x_1 - x_2)}{\Phi_2(f) - \Phi_1(f)} \quad (2)$$

Where f is the frequency; $\Phi_1(f)$ and $\Phi_2(f)$ are the phases of the signals recorded at point 1 and 2, which include the impulse response of the transducer and the other components in the test system. These addition unwanted contributions to the impulse response can be eliminated by subtracting $\Phi_1(f)$ from $\Phi_2(f)$, so that only the effect of measuring the $x_1 - x_2$ on phase shift remains. The data analysis is automatically given by software, an example is shown in Figure 2(b).

FIGURE 2 [HERE]

A pulsed nitrogen laser, with a wavelength of 337 nm, a pulse energy equal to 400 μJ and a pulse duration of 0.5 ns (peak power of 800 kW), was used. The ultrasonic wave was

detected using a steel knife edge acting on a 10 μm thick piezoelectric Polyvinylidene Fluoride film as a line detector. The piezoelectric signal was amplified, filtered, recorded by an oscilloscope, and processed. While an initial offset of about 5 mm between the laser and detector was used, the stage was moved by logarithmic steps between 5 and 50 mm. The software used to control, and process data was LAwave version 5.2.

3. Results and Discussion

3.1 Effect of surface topography and surface contact

The AFM results of the semiconducting SmS thin films with thicknesses of 100, 200 and 400 nm on the silicon substrate show low surface roughness. Figure 3 shows surface topography of a 400 nm thick SmS thin film. The average surface roughness (Ra), Rms roughness (Rq), and the maximum peak to valley height (Rp-v) were measured about 0.96, 1.18 and 5.17 nm, respectively. The low surface roughness reduces measurement uncertainties for nanoindentation, however, at the nano-scale, the surface contact still suffers from local variation in indentation depth.

FIGURE 3 [HERE]

FIGURE 4 [HERE]

Figure 4 shows the load-displacement curves obtained at very low loads on certified reference material (fused silica) and 400 nm SmS thin film with a 4.2 μm spherical indenter. The loading and unloading curves in Figure 4(a) do not overlap, despite that the material only

deforms elastically, as indicated in Figure 4(b). The mismatch gap is less than 2 nm, which is consistent with the surface roughness value of the fused silica, as the stress concentration causes plastic deformation within the range of roughness. The first few nanometres of permanent indentation depth in SmS thin films could also be due to the surface roughness causing high local stress and, therefore, local deformation rather than true plastic deformation of the thin film, as shown in Figure 4(c). There is true plastic deformation at an indentation load of about 0.22 mN (indicated by the small pop-in), Figure 4(d). The average contact pressure (in a range close to 650 MPa for different indents) at load of 0.3 mN could lead to a partial switch (the SmS switch from semi-conducting state to metallic state), but the maximum contact pressure could lead to permanent plastic deformation due to the non-uniform stress distribution below the indenter[23]. Despite the average surface roughness in the thin film being slightly lower than that of the reference material, the mismatch gap at the initial contact is up to 5 nm, which is close to the maximum peak to valley height. The difference could be caused by different plastic properties of the two materials, with fused silica being much harder than SmS thin film; and also may be due to the scratches introduced during polishing on fused silica, which could increase the average surface roughness. Therefore, despite the lower surface roughness, the local variation in the surface contact and associated high stresses highly likely to increase the nanoindentation measurement uncertainties at lower indentation depth; However, using a sharper cube corner indenter can reduce the effect of surface roughness and therefore, the measurement uncertainties at shallow indentation depths.

3.2 Elastic modulus measurement by nanoindentation

FIGURE 5 [HERE]

Figure 5 (a) shows the typical load-displacement curves obtained at the same maximum load on both silicon substrate and SmS thin films. The maximum indentation depth was found to increase with film thickness, which is an indentation effect observed when indenting a soft film on a stiffer substrate; the thinner the film the more significant the substrate effect at a given indentation load. Similar observations were made regarding the creep displacement at maximum indentation load.

During initial loading of the indenter, both elastic and plastic deformation occur; where plastic deformation occurs, the semiconductor phase switched to metallic phase, as presented in Figure 5(b). According to the improved Oliver-Pharr method [15], the unloading curve could be analysed by the concept of an 'effective indenter shape', as shown in lower part of Figure 5(b). The elastic unloading response is not from the plastic region under the indenter, but from the surrounding material. The effect of a silicon substrate on the elastic modulus of the thin film is strong, despite that the indentation depth is much lower than film thickness, which indicates that elastic response is mainly from the semiconducting phase and silicon substrate (after unloading, it is found that only the indent has a golden colour, corresponding to the metallic phase, insert in Figure 5(a)). The shape of the 'effective indenter' is the shape that would produce the same normal surface displacements on a flat surface to that produced by a cube corner indenter on the deformed surface. The successful determination of the effective indenter shape can be confirmed by overlapping the unloading and reloading curves [15, 24]. For the SmS thin films, no significant amount of hysteresis was observed during the reloading cycle, suggesting that the elastic recovery is mainly a combination of the SmS semiconducting phase and the substrate. Another common feature observed in Figure 5(a) for the force-displacement curve of thin film system is that there is a considerable amount of

displacement during the holding period at maximum load, which increases with indentation load and film thickness.

FIGURE 6 [HERE]

Figure 6(a) is a plot of the plane strain modulus of SmS thin films as a function of a/t (effective radius/film thickness). The plane strain elastic modulus of the film was determined to be 81 GPa (+/- 6 GPa) at shallow indentation depths of 20 nm (a/t is ~ 0.3) in the case of a 400 nm thick SmS film. The elastic modulus increases to 93 GPa (+/- 2 GPa) when decreasing the film thickness to 200 nm at a similar depth (a/t is ~ 0.6). The uptrend in the modulus of the films is the result of the elastic field under the indenter not being confined to the film itself; instead the elastic field extends into the substrate when indenting thin films. The elastic modulus increases with increasing the indentation depth (a/t ratio), reaching a value close to that of the silicon substrate. There is a definite substrate influence on the measured contact stiffness, even at shallow indentation depths, indicating that the rule of thumb of 10 % film thickness is invalid for the SmS thin films.

The experimental results compare favourably with a modified form of King's model [11, 13], which captures the substrate effect on the elastic modulus of thin films irrespective of pile up or sink in of materials. Within this model the elastic properties are related by

$$\frac{1}{E_r} = \frac{1-\nu_i^2}{E_i} + \frac{1-\nu_f^2}{E_f}\left(1 - e^{-\frac{\alpha(t-h)}{a}}\right) + \frac{1-\nu_s^2}{E_s}\left(e^{-\frac{\alpha(t-h)}{a}}\right) \quad (3)$$

where E_i, E_f and E_s are the elastic modulus of the indenter, film and substrate, respectively; E_r is reduced modulus; Poisson's ratio of the film and substrate are ν_f (0.21) [1, 25] and ν_s (0.22), respectively [4, 25]; the film thickness t and indentation depth h; a is the square root

of the projected contact area; α is a numerically determined scaling parameter that is a function of a/t, the normalized punch size, which depends on indenter geometries (cube corner and Berkovich).

We define $x = e^{-\frac{\alpha(t-h)}{a}}$ and $y = \frac{1}{E^*}(\frac{1}{1-\nu_f^2})$, where E^* is the plane strain modulus, $\frac{1}{E^*} = \frac{1}{E_r} - \frac{1-\nu_i^2}{E_i}$, where the Poisson ratios was taken as close to zero for Oliver & Pharr analysis. Hence, a linear fit defined by $y = Ax + B$, with

$A = \frac{1-\nu_s^2}{E_s(1-\nu_f^2)} - \frac{1}{E_f}$ and $B = \frac{1}{E_f}$, was established. The best-fit values of A and B can be determined using a linear least square method, and used to calculate the elastic modulus and Poisson's ratio of the SmS film.

Figure 6(b) shows plots of y versus x for SmS films with different thicknesses, where some points at indentation depth larger than thickness being excluded. For pure SmS thin films with uniform microstructure, the relationship of y vs. x is reasonably linear, indicating constant elastic properties for the 3 different film thicknesses. The Young modulus of thin film was extracted from the linear fitting (data from Figure 6(b)), which is the inverse of the interception with y axis, and summarised in table 1, along with the fitting coefficient R^2.

In addition, a near-linear range fitting of plane strain modulus vs a/t (a/t ratio is ≤ ~3.0, which is much larger than ISO recommendation of 1.5 [16] due to the availability of the data points) was attempted for three films (data from Figure 6(a)). The Young's modulus values are 73.4 +/- 2.34, 72.9 +/- 1.27 and 72.8 +/- 1.22 GPa for 100, 200 and 400 nm thin films, respectively; and they are at least 10 % lower than theoretical values. Despite good agreements for the intercepts of the fitting for the 3 films, the slopes of the fitting vary by ~20 % with different film thickness. As this fitting method aims to achieve linear fitting over a range of depths that do not creep and are elastic if possible [16], the large plastic and/creep

deformation in SmS thin films might affect the fitting results. Therefore, the King's model is recommended for sharp indenter on soft/ductile material.

Table 1 Young's modulus of SmS thin films with different thicknesses obtained from modified King's model of nanoindentation measurement, the LAwave method and theoretical values from literature.

Measured	**Fitted Modulus**		**LAwave**		**Literature**
Thickness (nm)	**(GPa)**	**R^2**	**(GPa)**	**St dev(GPa)**	**(GPa)**
424	78.7	0.85	88.4	3.0	80-90
197	82.0	0.93	86.0	3.5	[1, 4, 25]
102	81.3	0.88	90.6	6.6	

The effect of the different indenter shapes on the measurement of the elastic modulus was analysed. Figure 7 shows a typical plot of Young's modulus versus the indentation depth using a Berkovich indenter on a 400 nm thick SmS film. It is worth mentioning that the degree of variation in the experimental results obtained from Berkovich indents (Figure 7) performed at shallow depths is higher than those obtained from cube corner indents (Figure6 (a)), which is due to surface roughness effects previously discussed. The Oliver-Pharr method was used to calculate the combined elastic modulus, using a Poisson ratio of 0.21 for both the film and substrate and a modulus of 160 GPa for the silicon substrate[1, 4, 26]. The fitted Young modulus from the modified King model and Equation (3) matches well the experimental data obtained from the Oliver-Pharr method (Fig. 7) yielding a "film-only" elastic modulus of about 82.4 GPa (R^2 = 0.78).

FIGURE 7 [HERE]

3.3 LAwave results

Figure 8 shows the phase velocity of an acoustic wave for the 3 SmS film thicknesses, and the theoretical fits for the determination of the Young modulus. A Young modulus of about 90.4, 85.2 and 88.1 GPa was measured for the 100, 200 and 400 nm thick SmS films, respectively. The results were obtained from using a Poisson ratio of 0.21 [1, 2], an theoretical film density of 5.69 g/cm^3 and measured thicknesses of 102, 197 and 424 nm. A series of 8 measurements were made on each SmS thin film, and the results were averaged for each film, as summarised in table 1. Results from both the nanoindentation fitting using the modified King model and the LAwave technique are in a reasonable agreement with theoretical Young modulus values calculated from the elastic constants [1, 4, 25] , as shown in Table 1. The results give confidence in measuring Young's modulus of soft/ductile thin films with nanoindentation and LAwave when the size of specimen varies from sub-micrometre to millimetres, where theoretical elastic constants may not be available.

FIGURE 8 [HERE]

It was concluded that while the estimated Young's modulus values are highly dependent on the accuracy of the film thickness (an increase of 10% in thickness of 100 nm thick film, results in more than 50% increase of Young's modulus); they are less affected by the Poisson ratio. The accuracy of the film density also linearly affects the derived modulus; an increase of approximately 5 % in the density leads to a 50 % increase in the derived modulus. In this work, only Young's modulus was determined, while the density and film thickness were known and used as fixed values. While the bulk density was found in literature[2],

inspections of the film cross-sections under electron microscope were carried out to investigate any porosity and avoid an overestimation of the film density. According to current deposition process, it is expected the variation in thickness over 1 cm to be on the order of at most 0.2%, due to the characteristics of the technique, when the sample was situated right above the Sm source[19] . It is important to note that since the LAwave technique performs the measurement over a film area of approximately 5 mm by 10 mm, and assumes that the film is homogeneous, isotropic and of equal thickness, measurement uncertainties may arise from film non-uniformity.

4. Summary

Considering the nature (thin and soft/ductile) and size in potential application (sub-micrometre) of the SmS thin films, nanoindentation equipped with pyramid indenters (cube corner and Berkovich indenters) was used to measure the elastic modulus of semiconducting films with nominal thickness of 100 nm, 200 nm and 400 nm on silicon substrate at different loads. The total elastic strain generated during nanoindentation was not contained within the thin film, so the elastic properties obtained by the Oliver-Pharr method was a combination of the film and substrate. Therefore, we used a modified King's model, which enabled the determination of the "film-only" elastic modulus of SmS thin films while reaching indentation depths greater than 10 % of the film thickness. The results matched those obtained from the laser surface acoustic wave measurements as well as data calculated from literature. The combination of nanoindentation and LAwave measurements can increase confidence in the measurement accuracy of thin film modulus.

Acknowledgment

The authors acknowledge financial support from the Department of BEIS (Department for Business, Energy and Industrial Strategy) for funding, under the NMS (National Measurement System) program, and European Union's Horizon2020 research and innovation program within the PETMEM project (Grant Agreement No. 688282). Thank you to Vivian Tong (NPL) and Antony Thomas Fry (NPL) for internal review of the manuscript before submission.

Reference

[1] T. Hailing, G. A.Saunders, H. Bach, Elastic behavior under pressure of semiconducting SmS, Phys. Rev. B 29 (1984) 1848-1857.

[2] A. Sousanis, P. F. Smet, D. Poelman, Samarium Monosulfide (SmS): Reviewing Properties and Applications, Materials (Basel) 10 (2017) 953-973.

[3] P. M.Solomon, B. A.Bryce, M. A.Kuroda, R.Keech, S.Shetty, T. M.Shaw, M.Copel, L. W.Hung, A. G.Schrott, e. al, Pathway to the piezoelectronic transduction logic device, Nano Lett. 15 (2015) 2391-2395.

[4] V. V.Kaminskiy, N. N.Stepanov, N. M.Volodin, Y. N.Mishin, Baroresistor effect and semiconductor thin-film baroresistors based on samarium sulfide for spacecraft applications, Sol. Syst. Res. 48 (2014) 561-567.

[5] Y. F. Cao, S. Allameh, D. Nankivil, S. Sethiaraj, T. Otiti, W. Soboyejo, Nanoindentation measurements of the mechanical properties of polycrystalline Au and Ag thin films on silicon substrates: Effects of grain size and film thickness, Mater. Sci. Eng. A 427 (2006) 232-240.

[6] R. D. Jamison, Y. L. Shen, Indentation-derived elastic modulus of multilayer thin films: Effect of unloading-induced plasticity, J. Mater, Res. 30(15) (2015) 2279-2290.

[7] K. Vanstreels, C. Wu, M. Gonzalez, D. Schneider, D. Gidley, P. Verdonck, M. R. Baklanov, Effect of pore structure of nanometer scale porous films on the measured elastic modulus, Langmuir 29 (2013) 12025-12035.

[8] H. Li, J. J. Vlassak, Determining the elastic modulus and hardness of an ultra-thin film on a substrate using nanoindentation, J. Mater. Res. 24 (2011) 1114-1126.

[9] C. A.Clifford, M. P.Seah, Nanoindentation measurement of Young's modulus for compliant layers on stiffer substrates including the effect of Poisson's ratios, Nanotechnology 20 (2009) 145708-145716.

[10] H. Y. Chung, M. B. Weinberger, J. M. Yang, S. H. Tolbert, R. B. Kaner, Correlation between hardness and elastic moduli of the ultraincompressible transition metal diborides RuB2, OsB2, and ReB2, Appl. Phys. Lett. 92 (2008) 261904-261907.

[11] S. Ranjana, W.D. Nix, Effects of the substrate on the determination of thin film mechanical properties by nanoindentation, Acta Mater. 50 (2002) 23-38.

[12] S. Suresh, T. G. Nieh, B.W. Choi, nano-indentation of copper thin films on silicon substrates, Scrip. Mater. 41 (1999) 951-957.

[13] R. B.King, Elastic analysis of some punch problems for a layered medium, Int. J. Sol. Struc. 23 (1987) 1657-1664.

[14] T. Chudoba, M. Griepentrog, A. Duck, D. Schneider, F. Richter, Young's modulus measurments on ultra-thin coatings, J. Mater. Res. 19 (2004) 301-314.

[15] G.M.P. W.C. Oliver. Measurement of hardness and elastic modulus by instrumented indentation advances in understanding and refinements to methodology, J. Mater. Res. 19 (2004) 3-22.

[16] Mettalic Materials--instrumented indentation test for hardness and materials parameters Part 4: Test method for metallic and non-metallic coatings, BSI Standards Publication (BS EN ISO 14577-4: 2016) (2016) 30.

[17] X. B. Feng, J. U. Surjadi, X. C. Li, Y. Lu, Size dependency in stacking fault-mediated ultrahard high-entropy alloy thin films, J. Alloys Comp. 844 (2020) 156187-156196.

[18] Z. L. Dong, Y. F. Peng, Z. Q. Tan, G. L. Fan, Simultaneously enhanced electrical conductivity and strength in Cu/graphene/Cu sandwiched nanofilm, Scrip. Mater. 187 (2020) 296-299.

[19] A. Sousanis, D. Poelman, C. Detavernier, P. F. Smet, Switchable Piezoresistive SmS Thin Films on Large Area, Sensors (Basel) 19 (2019) 4390-4402.

[20] S. Berezina, P. V. Zinin, D. Schneider, D. Fei, D.A. Rebinsky, Combining Brillouin spectroscopy and laser-SAW technique for elastic property characterisation of thick DLC films, Ultrasonics 43 (2004) 87-92.

[21] D. Schneider, T. Witke, T. Schwarz, B Schoneich, B. Schultrich, Testing ultra-thin films by laser-acoustics, Surf. Coat. Tech. 126 (2000) 136-141.

[22] D. Schneider, C. F. Meyer, H. Mai, B Schoneich, H Ziegele, H J Scheibe, Y. Lifshitz, Non-destructive characterisation of mechanical and structural properties of amorphous diamond-like carbon films, Diam. Relat. Mater 7 (1998) 973-979.

[23] K.L. Johnson, Contact Mechanics, Cambridge University Press, Cambridge, 1985.

[24] J. P. Sun, C. Li., H. Jiang, A. B. Ma, F. Liang, Nanoindentation Induced Deformation and Pop-in Events in a Silicon Crystal: Molecular Dynamics Simulation and Experiment, Sci. Rep. 7 (2017) 10282-10293.

[25] E. G.Soboleva, A. Ingisheva, T. B.Krit, Elastic Properties of Solid Solutions with Intermediate Valence Sm_{1-x}Y_xS, Appl. Mech. Mater. 770 (2015) 137-143.

[26] S. Raymond, J. P. Rueff, M. D'Astuto, D. Braithwaite, M. Krisch, J. Flouquet, Phonon anomalies at the valence transition of SmS: An inelastic x-ray-scattering study under pressure, Phys. Rev. B 66 (2002) 220301-220304.

Figure List

Figure 1 (a) Schematic of indentation; (b) corresponding load-displacement curve.

Figure 2 (a) Schematic of the ultrasonic measurement process, (b) example showing the effect of film on the phase velocity of the surface acoustic wave as a function of frequency.

Figure 3 AFM scan of SmS 400 nm thin film surface: (a) 3D topography, (b) the associated topographical line profile acquired along the dashed arrow in (a).

Figure 4 Load-displacement indentation curves carried out at very low loads with a spherical indenter with a radius of 4.2 μm to demonstrate the effect of surface roughness on indentation depth of fused silica at a maximum load of 0.05 mN and 2 mN (a and b, respectively); and on SmS 400 nm film with a maximum load of 0.05 mN and 0.3 mN (c and d, respectively).

Figure 5 (a) Load-displacement curves of silicon (100) substrate and SmS thin films with varying thickness using a cube corner indenter and the inserted optical image of an indent (yellow, at maximum load of 5 mN with an Berkovich indenter, width of insert is 10 μm) on 200 nm SmS film (purple ; and (b) schematics to understand the loading and unloading deformation of the film.

Figure 6 (a) Plane strain modulus of SmS thin films on silicon substrate plotted as a function of the a/t ratio (effective radius/film thickness) - the shaded pattern indicates the elastic modulus of silicon substrate; (b) a plot of $y = \frac{1}{E^*}\left(\frac{1}{1-\nu_f^2}\right)$ versus $x = e^{-\frac{\alpha(t-h)}{a}}$ (the x and y parameters are based on a modified King's model, which are explained in the text) for SmS thin films with different thicknesses – the dashed lines indicate linear fitting and plateau.

Figure 7 Young's modulus data obtained from the Oliver-Pharr method on Berkovich indents on 400 nm thick film and a fit using the modified King model.

Figure 8 Phase velocity of an acoustic wave as a function of frequency for SmS films with different thicknesses.

Fig. 1

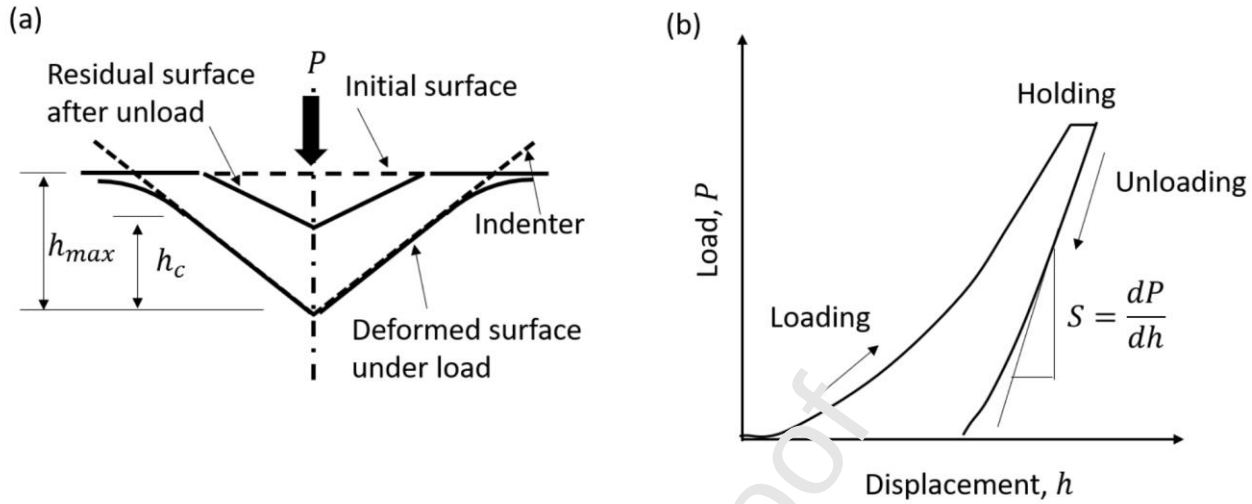

Fig. 2

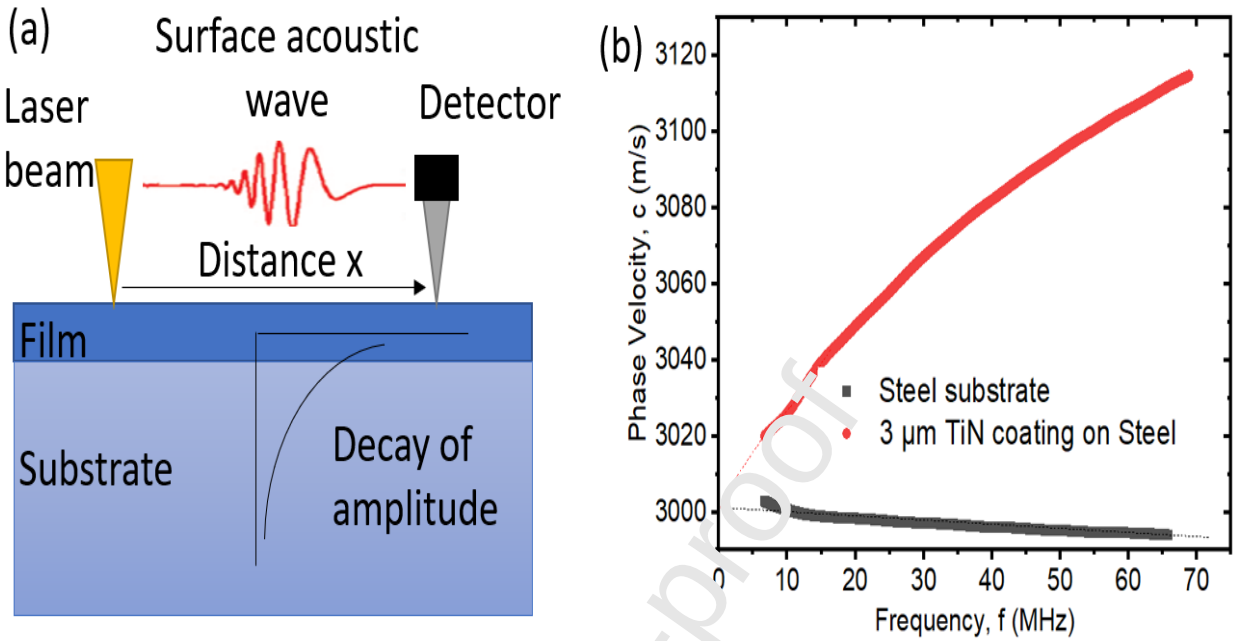

Fig. 3

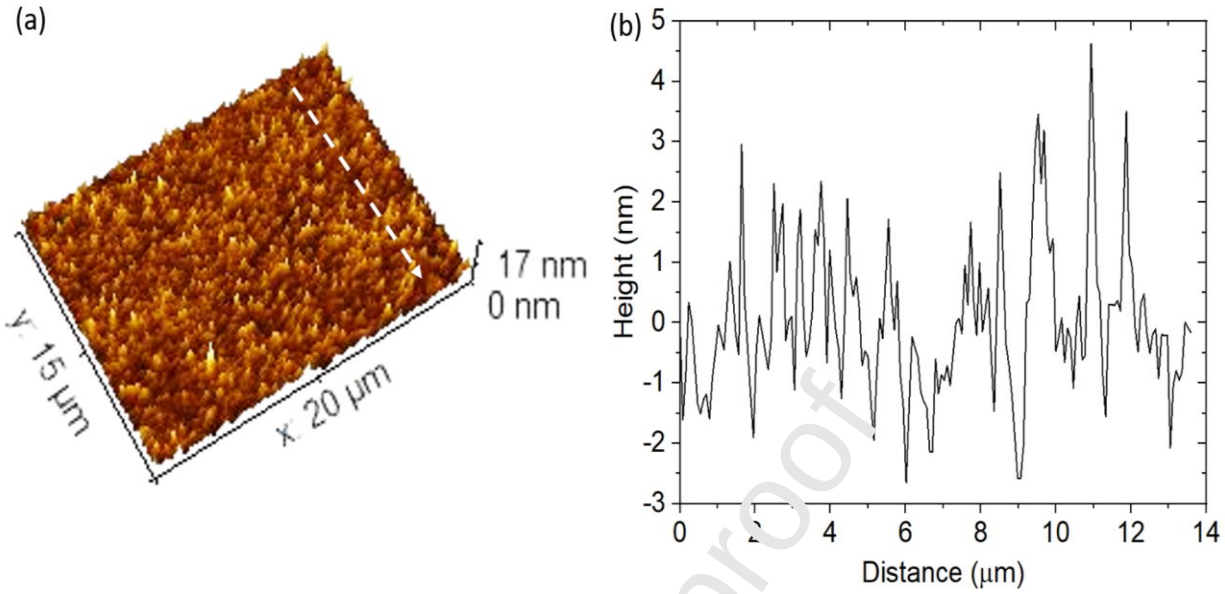

Fig. 4

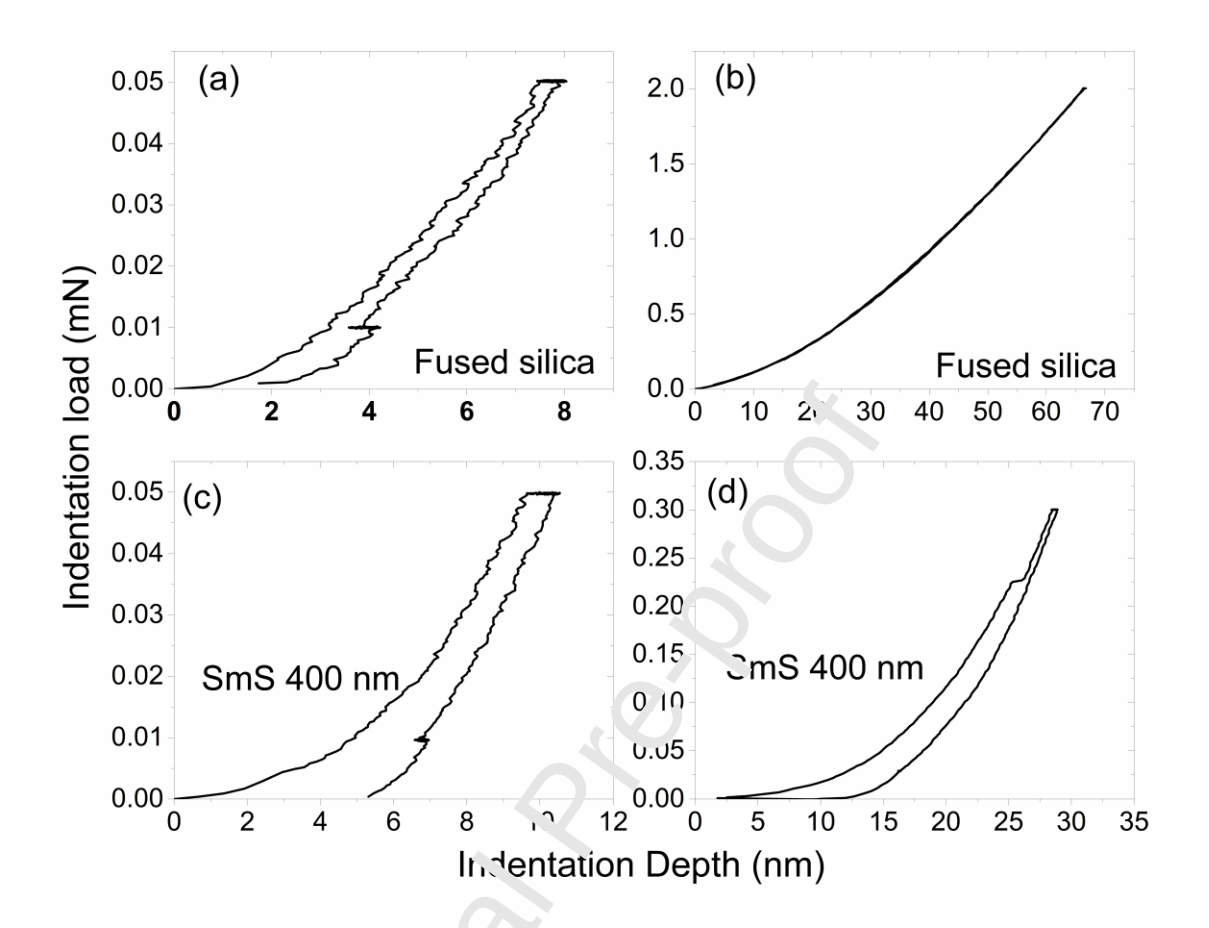

Fig. 5a

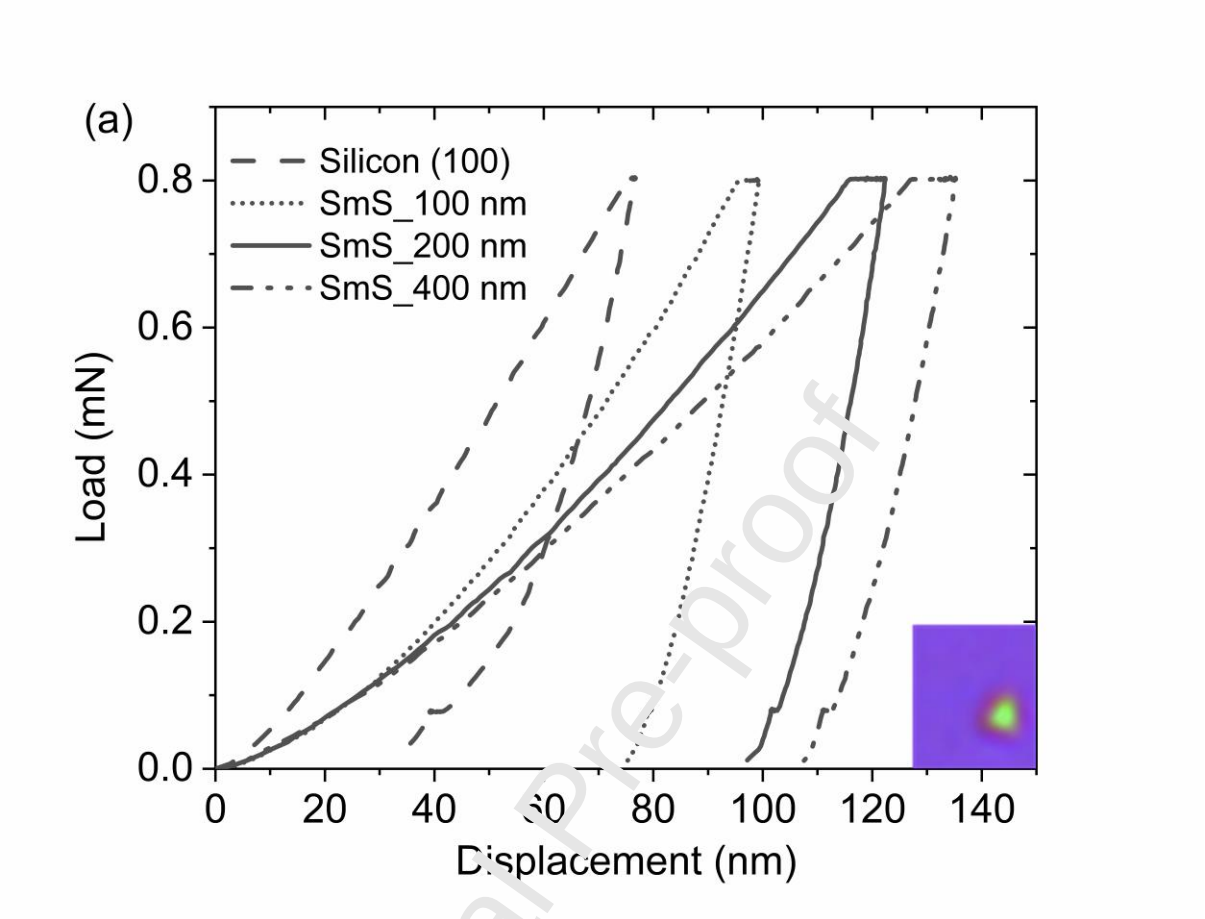

Fig. 5b

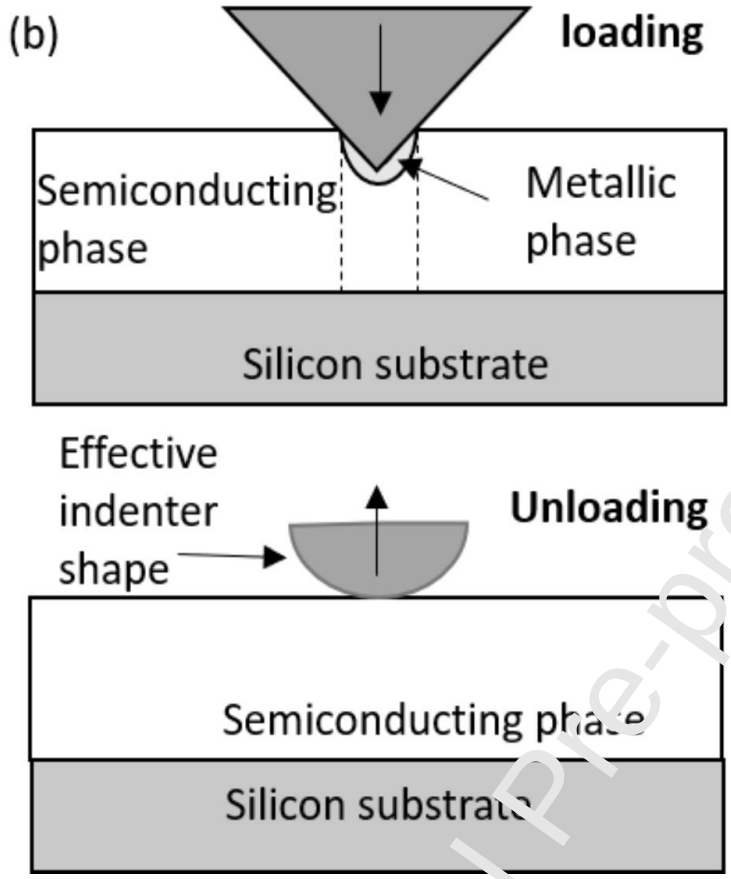

Fig 6a

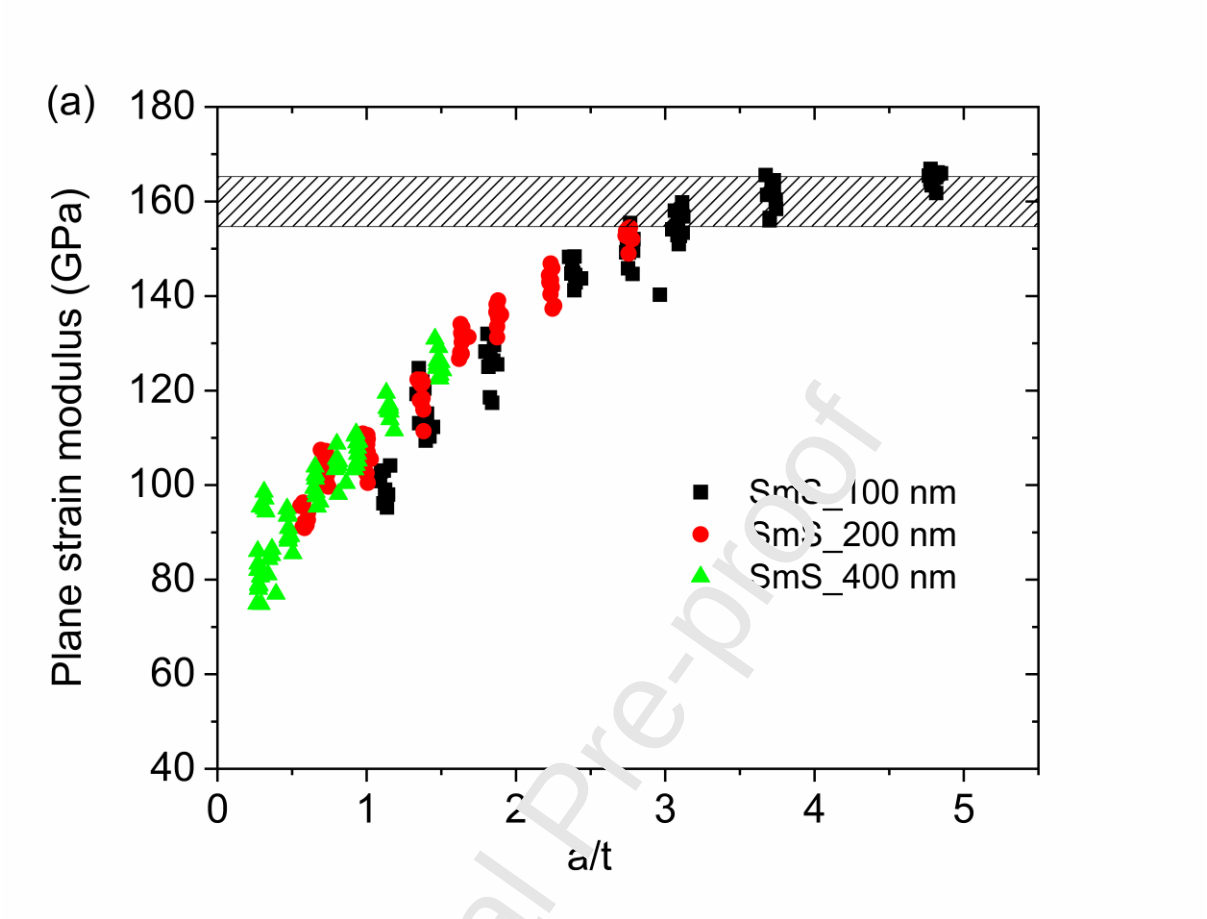

Fig. 6b

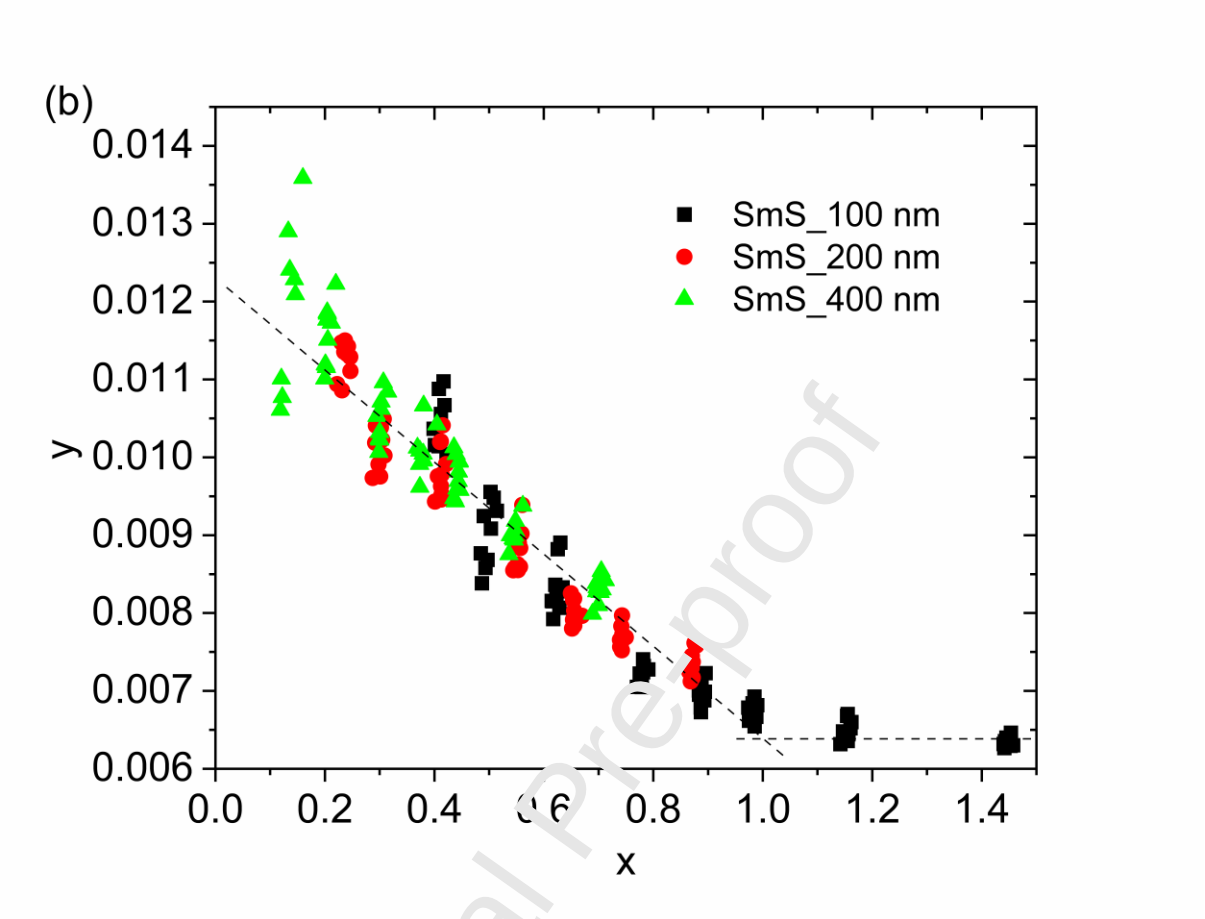

Fig.7

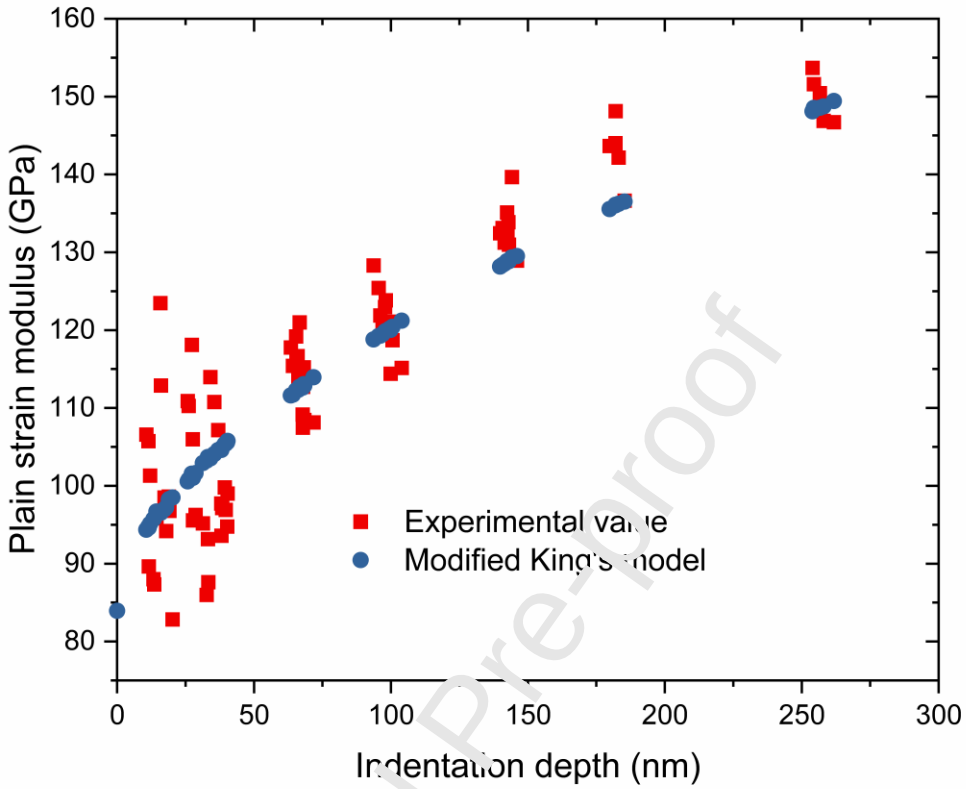

Fig. 8

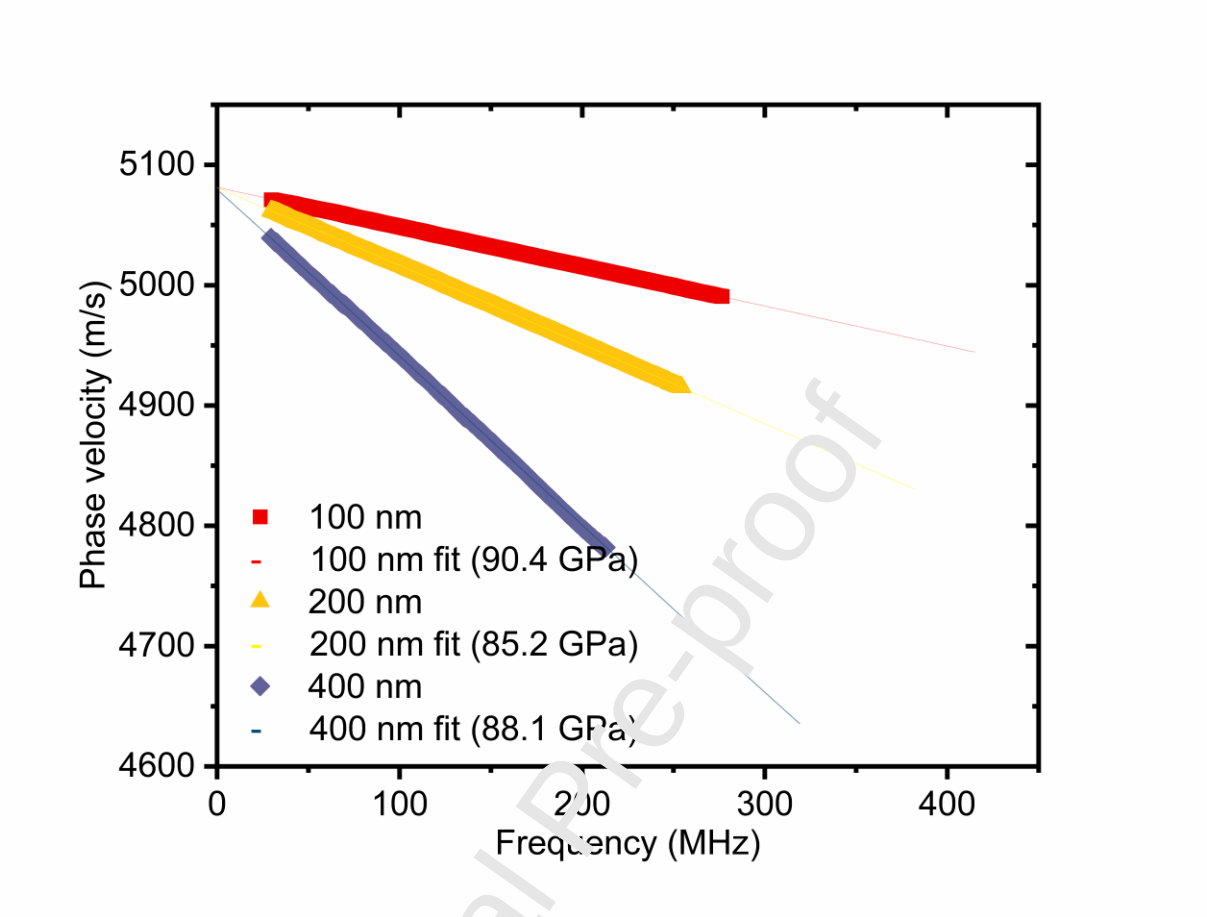

Credit author statement

IR led the collaboration between Ghent University and NPL; DFS, AS and DP prepared thin films; MS performed LAwave tests and data analysis; HZ performed nanoindentation test, AFM imaging and data analysis with input from FDL and MG. HZ drafted the manuscript with contributions from all authors in the writing and discussions.

Declaration of interests

☒ The authors declare that they have no known competing financial interests or personal relationships that could have appeared to influence the work reported in this paper.

☐The authors declare the following financial interests/personal relationships which may be considered as potential competing interests:

Highlights

Young's modulus of piezoresistive samarium sulphide thin films was measured.

The modified King's model was used to fit nanoindentation results.

Laser surface acoustic wave was used to measure Young's modulus directly.

Different experimental results match with theoretical values from literature.

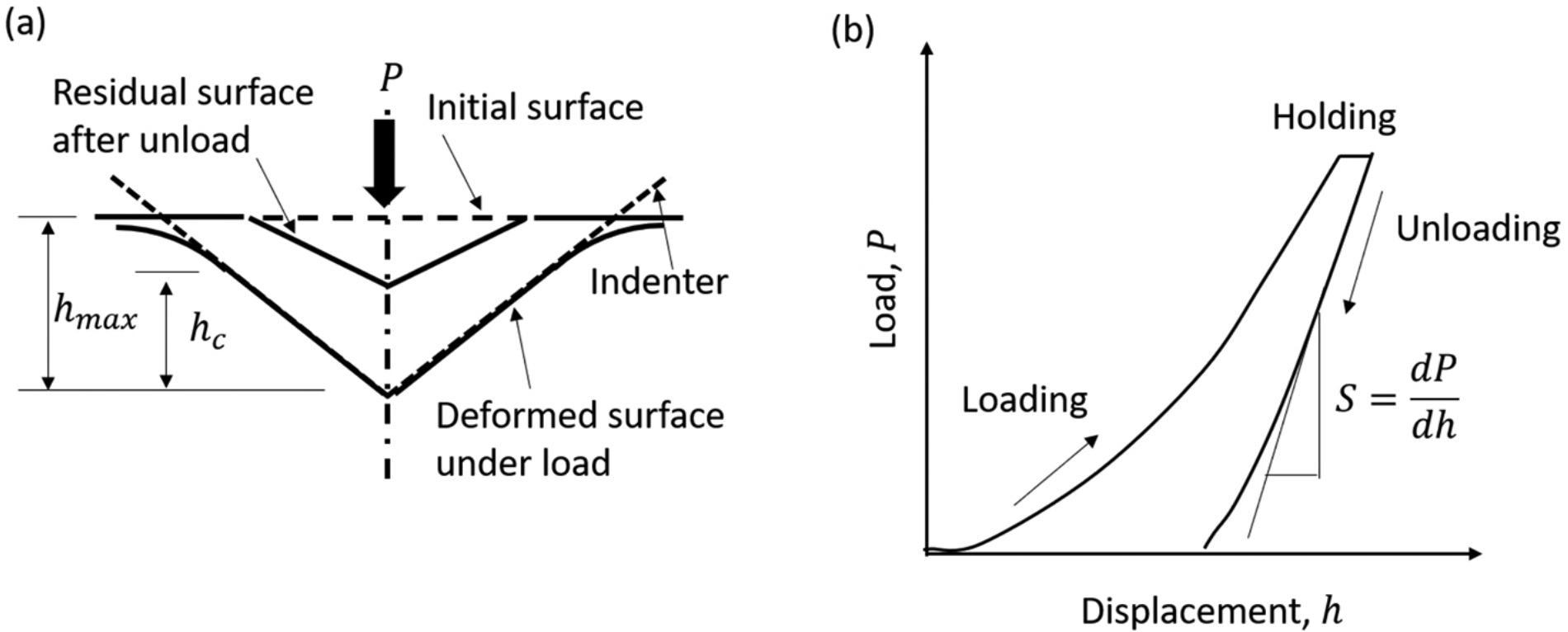
(a)
Residual surface
after unload
P
Initial surface
Indenter
h_{max}
h_c
Deformed surface
under load
(b)
Holding
Unloading
Load, P
Loading
$S = \frac{dP}{dh}$
Displacement, h

Figure 1

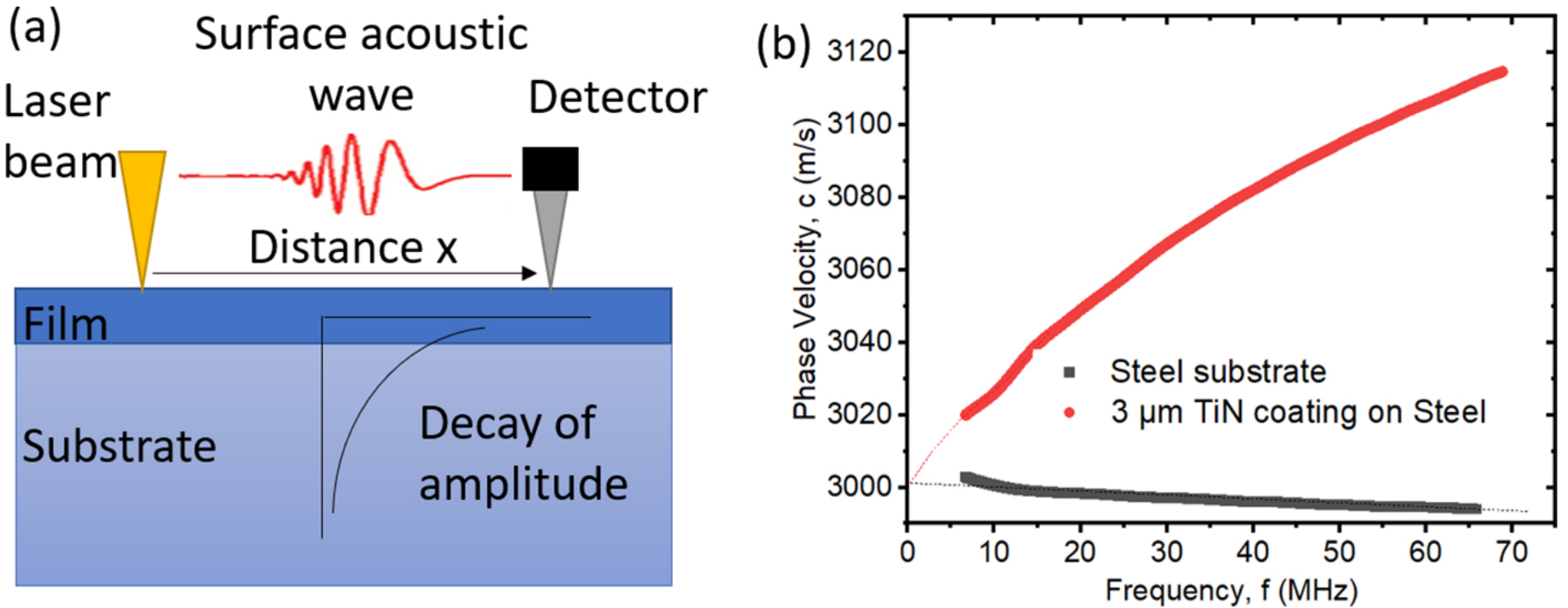
(a)
Surface acoustic wave
Laser beam
Detector
Distance x
Film
Substrate
Decay of amplitude
(b)
Phase Velocity, c (m/s)
3120
3100
3080
3060
3040
3020
3000
0
10
20
30
40
50
60
70
Frequency, f (MHz)
Steel substrate
3 μm TiN coating on Steel

Figure 2

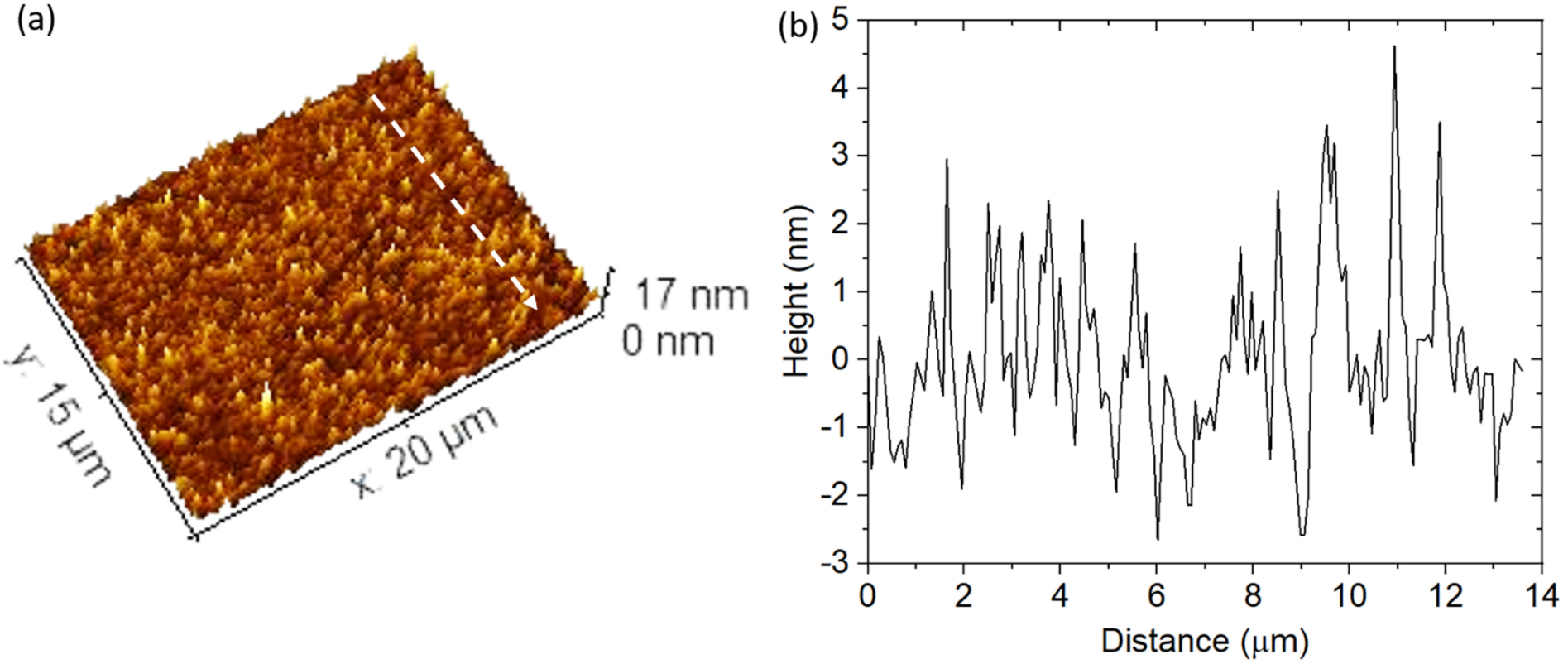
(a)
17 nm
0 nm
Y: 15 µm
X: 20 µm
(b)
Height (nm)
Distance (µm)
5
4
3
2
1
0
-1
-2
-3
0
2
4
6
8
10
12
14

Figure 3

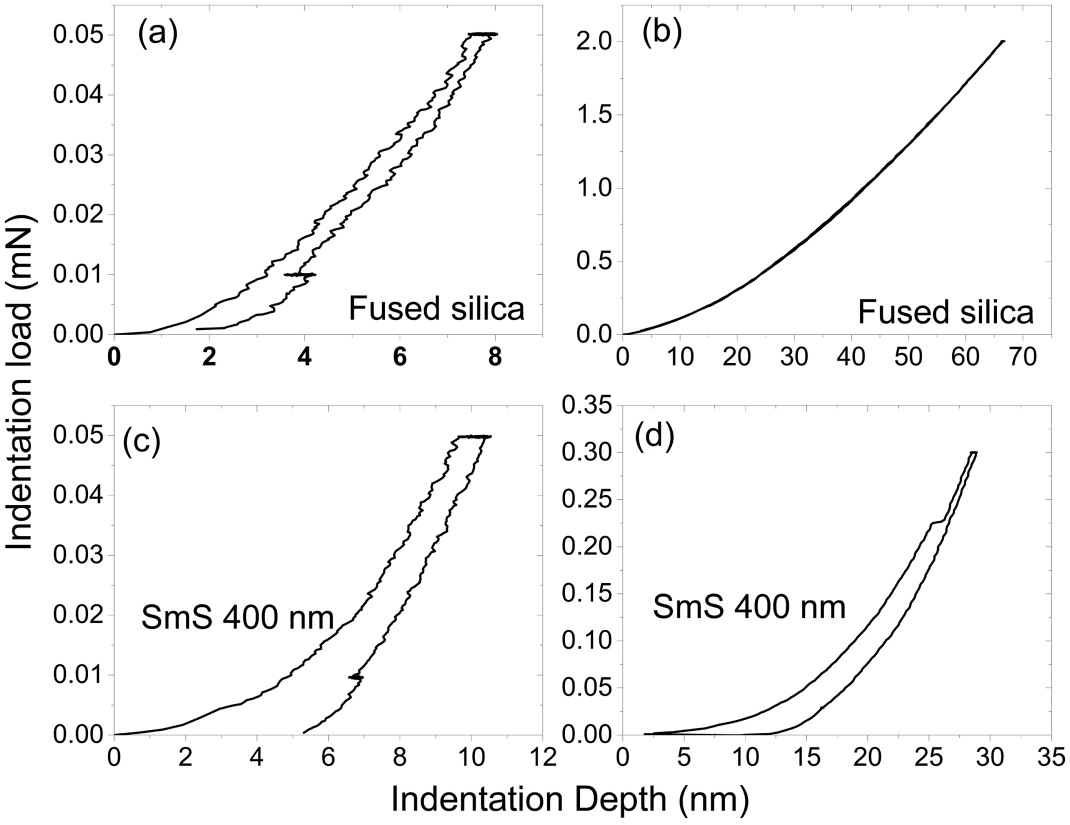
(a)
Fused silica
(b)
Fused silica
(c)
SmS 400 nm
(d)
SmS 400 nm
Indentation load (mN)
Indentation Depth (nm)

Figure 4

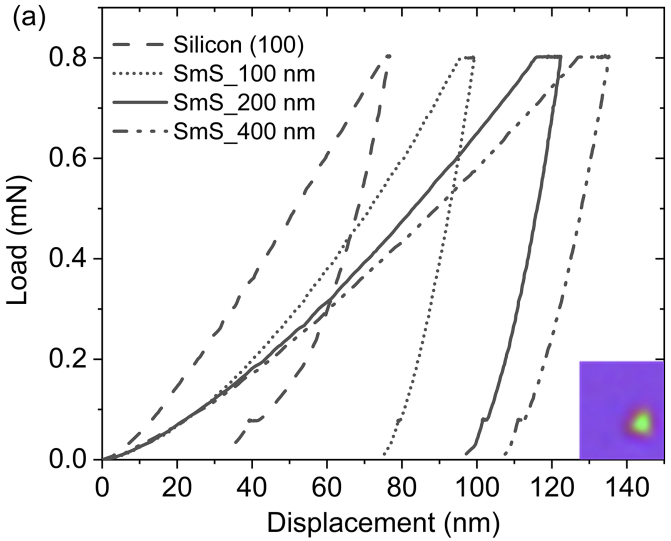
(a)
Silicon (100)
SmS_100 nm
SmS_200 nm
SmS_400 nm
Load (mN)
0.0
0.2
0.4
0.6
0.8
0
20
40
60
80
100
120
140
Displacement (nm)

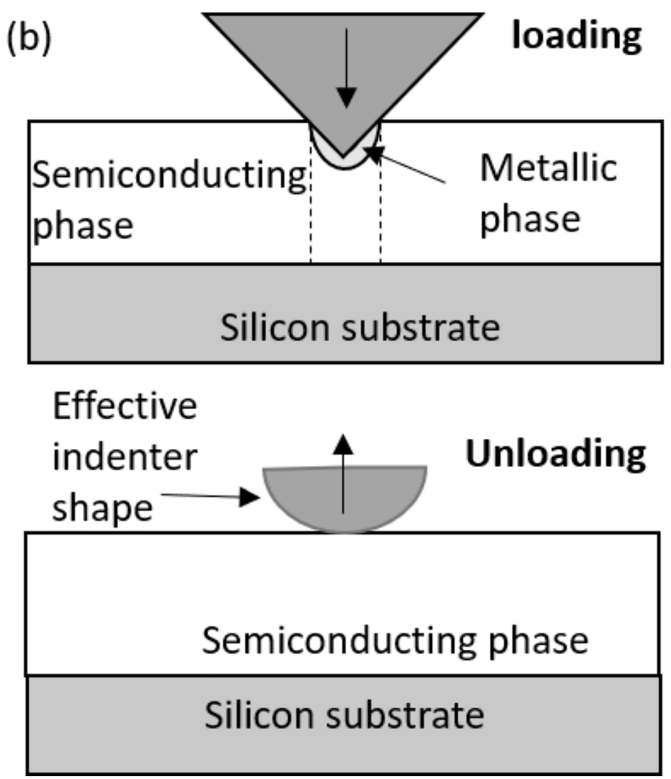
(b)
loading
Semiconducting phase
Metallic phase
Silicon substrate
Effective indenter shape
Unloading
Semiconducting phase
Silicon substrate

Figure 5

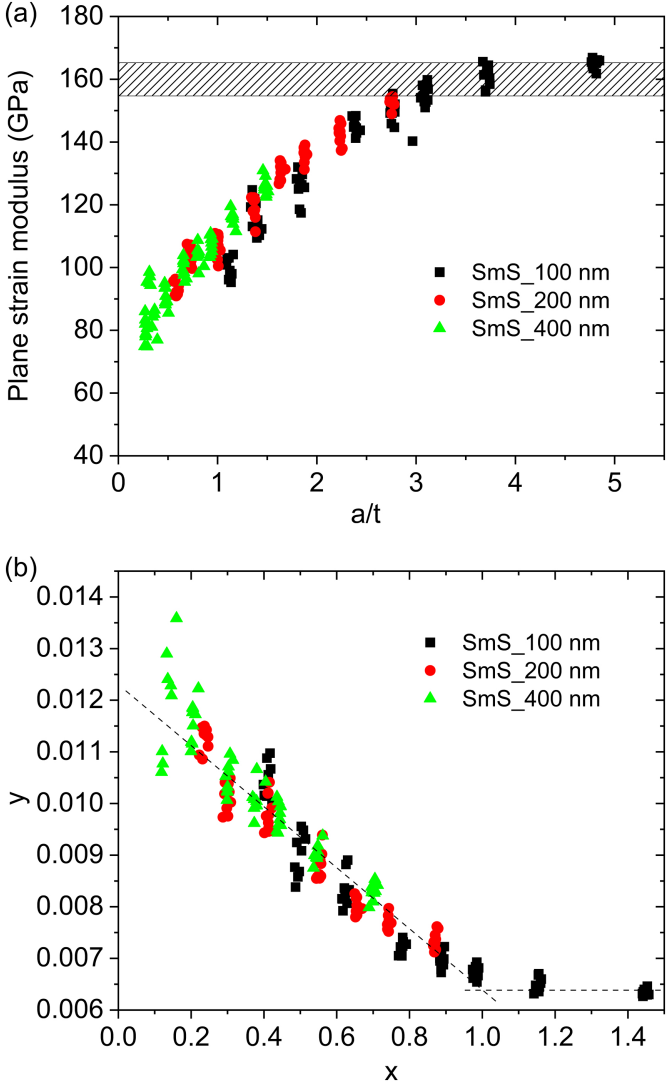
(a)
Plane strain modulus (GPa)
a/t
SmS_100 nm
SmS_200 nm
SmS_400 nm
(b)
y
x
SmS_100 nm
SmS_200 nm
SmS_400 nm

Figure 6

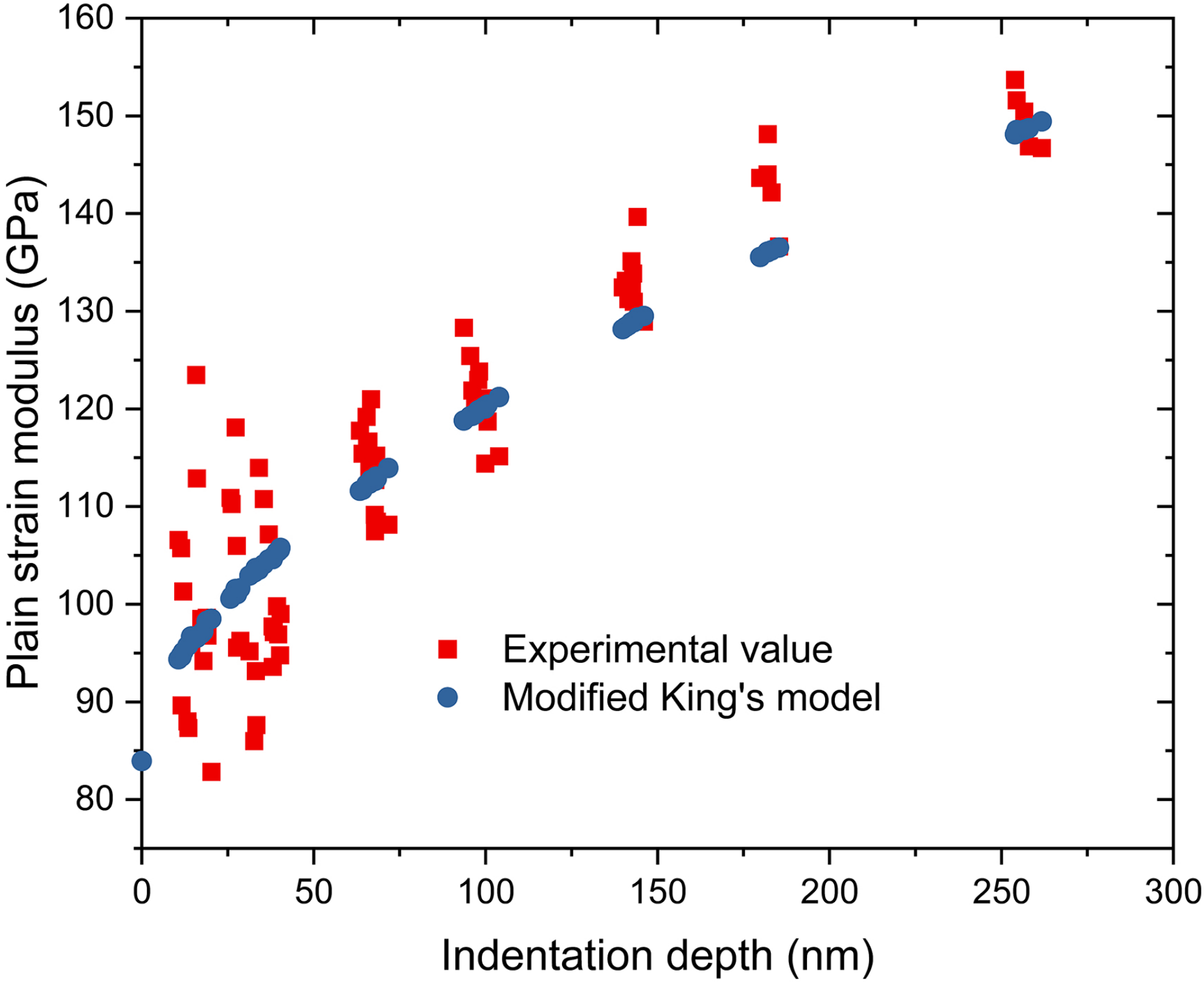
Plain strain modulus (GPa)
160
150
140
130
120
110
100
90
80
0
50
100
150
200
250
300
Indentation depth (nm)
Experimental value
Modified King's model

Figure 7

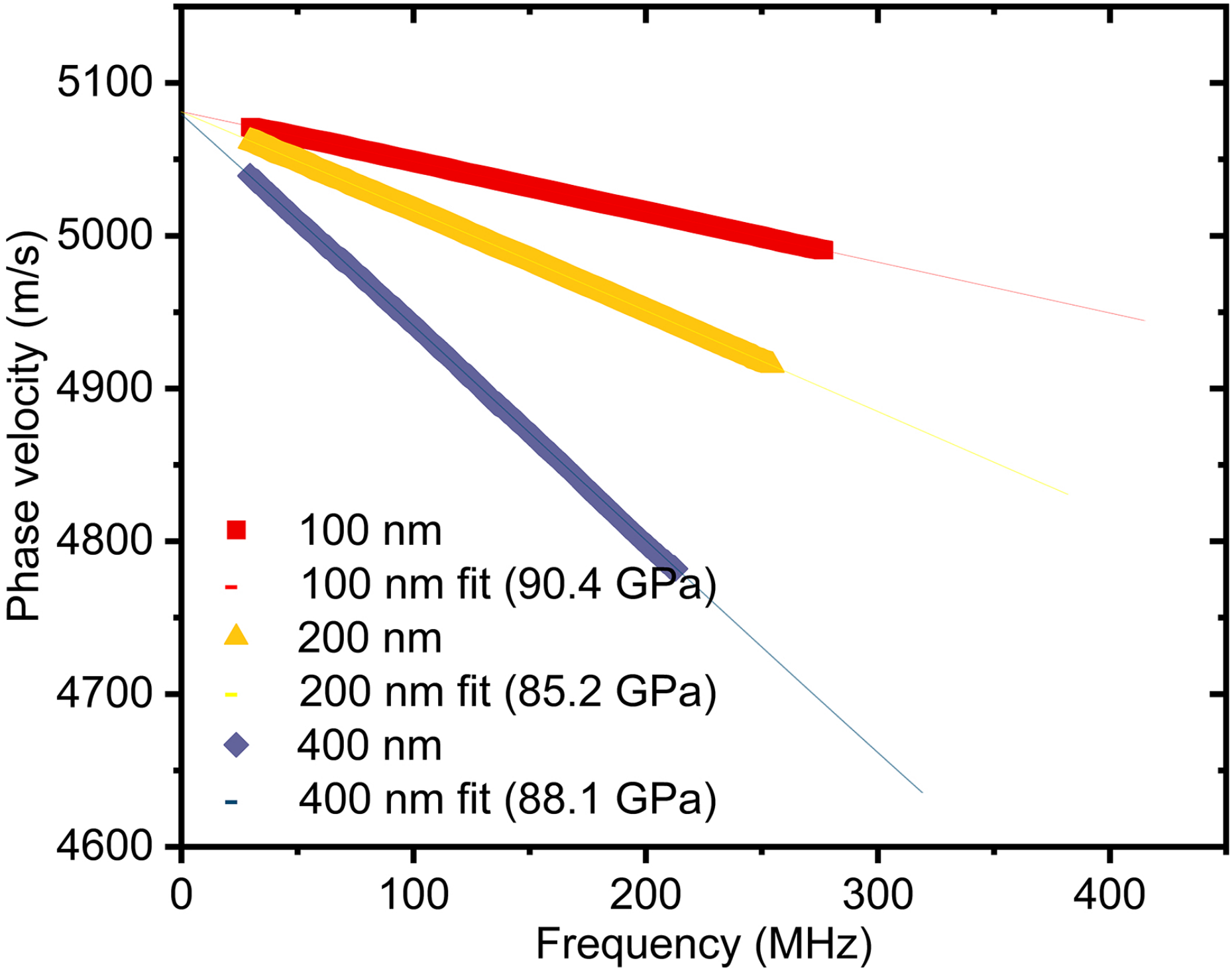
5100
5000
4900
4800
4700
4600
Phase velocity (m/s)
0
100
200
300
400
Frequency (MHz)
100 nm
100 nm fit (90.4 GPa)
200 nm
200 nm fit (85.2 GPa)
400 nm
400 nm fit (88.1 GPa)

Figure 8